Energy Equip. Sys./ Vol. 11/No. 3/September 2023/ 339-351

ENERGY EQUIPSYS

Energy Equipment and Systems
http://energyequipsys.ut.ac.ir
www.energyequipsys.com

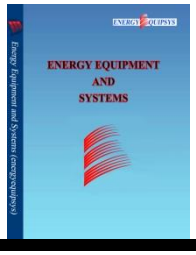

Utilizing Blast Furnace gas to run a supercritical CO_2 cycle to meet part of the internal consumption of the iron plant and to produce fresh water through a multi-effect desalination unit

Authors

Ali Fallah Ardashir[a*]
Faramarz Ranjbar [a]
Mortaza Yari [a]

[a]Department of Mechanical Engineering, Faculty of Mechanical Engineering, University of Tabriz, Tabriz, Iran

Article history:

Received : 9 May 2023
Accepted : 5 June 2023

ABSTRACT

Iron furnace gases, a byproduct of the steel and iron industries, have been the subject of research on employing them to power some of the factory's internal needs. The rise in fuel costs and focus on energy system sustainability have created distinct frameworks for heat loss sources and low-value fuels. In this study, iron furnace gas produced in steel and iron factories has been used to produce additional power to provide part of the domestic power consumption of these factories. The supercritical carbon dioxide cycle has been used to generate power. The results show that at the optimal point, the system has emissions of 0.52 and a net power output of 22100 kWh. Also, the system's efficiency is 38.56% and carbon dioxide emission is 0.510 tons/MWh. Also, by increasing the exhaust gas temperature by 150 degrees, it is clear that 2 MW of recycled heat can be obtained. Also, in this regard, the output work of the turbine has increased by 0.8 kW and increases the efficiency of the whole cycle by 31.5% to 37%.

Keywords: Supercritical Carbon Dioxide Cycle, Steel Plant, Blast Furnace, Multi-Effect Desalination Unit.

1. Introduction

Since the Industrial Revolution until today, many waste gases have been produced in iron and steel facilities. These gases increase energy consumption and are unsafe by releasing CO_2. Different frameworks for heat loss sources have been devised as a result of the increase in fuel prices and the emphasis on energy system sustainability.

In order to increase energy conversion efficacy and reduce CO_2 emissions in iron-steel facilities, thermodynamic analysis methods must be applied to such thermal systems. Numerous energy-saving and emission-reduction measures, including raw materials substitution, waste heat recovery, power production, and CO_2 fixation, have been evaluated using economic and energy-related indicators. In addition, it is crucial to understand the thermodynamic efficiencies of the power-generating systems that utilize the useful waste gases produced by iron-steel facilities. Unfortunately, few articles have addressed the specifics of thermodynamic analysis of iron/steel production processes in iron-steel

* Corresponding author: Ali Fallah Ardashir
Department of Mechanical Engineering, Faculty of Mechanical Engineering, University of Tabriz, Tabriz, Iran
ardashir.ali@gmail.com

plants. The blast furnace boiler system was studied by Zetterholm et al. [1] in order to quantitatively assess its performance. The consequences of re-burning the blast furnace gas that was exhausted from the boiler system after the process was investigated to save natural gas, particularly the coke gas used to power the blast furnace boiler, which is one of the LPG fuels. Açkkalp et al. [2] assessed the thermodynamic performance of the CCPP built at Turkey's Eskisehir which consists of a gas cycle utilizing natural gas as fuel, a steam cycle, and HRSG. They indicated that the gas turbine and combustion chamber are parts of the upgrade priority utilizing the improved exergy analysis. By using an improved exergy analysis, Boyaghchi, and Molaie [3] assessed the thermodynamic performance of a combined cycle power plant made up of an HRSG and duct burner that consumes natural gas. In their study, it was examined how the performance of the aforementioned system and its constituent parts was impacted by the turbine input temperature and compressor pressure rate. Anvari et al. [4] evaluated a CCPP with HRSG utilizing natural gas for power, heating, and cooling from a thermal and financial point of view. They did this using an enhanced-exergy-based study. So, they conducted an optimization study to increase energy efficiency and decrease production costs. As the literature and the foregoing research are properly scrutinized, it is apparent that iron-steel factories must recycle valuable waste gases to reduce energy consumption and environmental pollution.

The supercritical CO_2 Brayton cycle was proposed for the first time in 1948 by Sulzer, and after that much research has been done on this cycle. Fehr was one of the people who provided valuable information in this field. The first CO_2 cycle was proposed by Fehr in 1967. The revitalization cycle proposed by him worked completely above the critical pressure of CO_2 and the cycle was regenerative and the condensing process was performed in the liquid phase. The S-CO_2 cycle was compared to helium-gas and water-steam-based cycles by Dostal et al. [5], who came to the conclusion that the S-CO_2 cycle was adequate if the output temperature is more than 550 ℃ in the reactor core. Because the heat source temperature has a limited range, the S-CO_2 cycle allows for simple system optimization and control. The direct S-CO_2 cycle offers a better overall efficiency for applications in concentrated solar power (CSP). The advantage is accompanied by an increase in thermal storage costs [6].

Numerous studies have concentrated on evaluating the effectiveness of desalination technologies. A MED system was evaluated for wastewater desalination in research by Zhao et al. [7]. More MED stages are found to be energy-efficient, but the capital expense is considerable. A numerical analysis of a ZLD system made up of an evaporative crystallizer and a MED unit was done by Chen et al. [8]. They discovered that the ZLD system's second law efficiency ranges from 10% to 17% and that if waste heat is available, the overall cost may be decreased to 1.16 USD/m^3. The particular energy consumption of the ZLD system may be significantly decreased with an upgrade to the MED system and energy-efficient integration. Many changes and improvements to the MED design have been suggested in recent years to increase energy efficiency, including the use of adsorption vapor compression [8] and absorption vapor compression [9]. The present working range of MED, which can accommodate 8–10 evaporators, is 40–65 °C [10]. This range is constrained by ambient conditions and scaling limits. Chitgar and Emadi [11] suggested an inventive multi-generation system, finding that the MED unit with an hourly output of 5.6 m^3 is the best choice for potable water generation from low-temperature exhaust gases. Aguilar-Jimenez et al. [12] evaluated and contrasted the impact of adding a MED unit for using the waste heat of a low-temperature heat source, achieving a greater performance efficiency of 22% in comparison to the single-generation power cycle. Marques et al. [13] examined a unique trigeneration system from the thermodynamic side. They came to the conclusion that the thermochemical hydrogen cycle and the MED unit, respectively, are used to create the additional 5 kg/s and 980 kg/s of hydrogen and drinkable water.

According to the systems described in the literature, the main problem with these systems is that they are not as efficient as more complicated systems. Another problem is that factories, especially steel factories, waste a lot of energy that can't be used effectively.

Nomenclature

C	Compressor
$\dot{E}$	Exergy rate (kW)
h	Specific enthalpy (kJ/kg)
HTR	High temperature recuperator
is	Isentropic
LHV	Lower heating value
LTR	Low temperature recuperator
P	Pressure (kPa)
$\dot{Q}$	Heat (kW)
R_p	Pressure ratio
T	Temperature (°C)
Subscript and abbreviations	
MED	Multi-effect desalination unit
$S\text{-}CO_2$	Supercritical carbon dioxide
TIT	Turbine inlet temperature
Greek symbols	
η_I	First law efficiency
η_{ex}	Second law efficiency

2. System description

The proposed system is shown as a schematic diagram in Fig. 1. In this cycle, the fluid flow in heat exchanger 1 receives heat and leaves it with the maximum temperature of the cycle (state 3). The fluid flow enters the turbine and with its expansion, it produces power. which is converted into electrical energy by the generator. The output flow from the turbine first enters the high-temperature recuperator (4-5) and then the low-temperature recuperator (5-6) and loses its heat and its temperature decreases. The output stream from the low-temperature recuperator is divided into two parts (state 6). Flow 7a with high mass flow rate and flow 7b with low mass flow rate. Before entering compressor 1, flow 7a loses its heat in the precooler and its temperature decreases, and then it is compressed in compressor 1 to the high pressure of the cycle (8-9). The output flow from compressor 1 is heated in the low-temperature recuperator and its temperature increases. The other part of the flow in compressor 2 is compressed to the high pressure of the cycle and after leaving compressor 2, it is mixed with the main flow coming out of the low-temperature recuperator, and then the mixture of the two flows enters the high-temperature recuperator. The exhaust gases are still valuable to run a MED system, therefore the exhaust gases from heat exchanger 1 enter into the heat recovery steam generator (HRSG) unit to start the desalination system. The steam ejector and flash boxes make up the heat-driven MED system. The secondary vapor from the final stage is combined with the main steam with a high enthalpy in the ejector. The first stage's heat source is made up of the produced superheated steam, which has a mean pressure. Seawater is shared equally across the stages as the feedwater. To reach the boiling point of the feedwater in the first stage, heat is transferred from the superheated steam to it. As a heat source for the evaporation process in the second step, the created steam is used. The residual brine then enters the next cycle to enhance system performance and produce additional vapor. In order to mix with the created vapor, a little portion of condensed vapor is also briefly re-evaporated under a lower pressure. In order to create the ideal potable water, this procedure is repeated.

3. Materials and methods

3.1 Thermodynamic assessment

To obtain the flow of mass and energy in each of the system's constituent parts, the mass and energy balances are stated as

$$\sum \dot{m}_{in} = \sum \dot{m}_{out}\,, \tag{1}$$

$$\dot{Q} - \dot{W} = \sum \dot{m}_{out} h_{out} - \sum \dot{m}_{in} h_{in}\,. \tag{2}$$

The exergy balancing equation is also used to compute the amount of exergy destroyed in each component of the system is given by [14].

$$\dot{E}_Q - \dot{E}_W = \sum \dot{m}_{out} e_{out} - \sum \dot{m}_{in} e_{in} + \dot{E}_D,\,. \tag{3}$$

where $\dot{Q}$ and $\dot{W}$ denote the heat transfer rate and power rate to and from the control volume, respectively. Also $\dot{E}_D$ is the rate of exergy destruction in the control volume, while $\dot{E}_Q$ and $\dot{E}_W$ are the rates of exergy transfer associated with $\dot{Q}$ and $\dot{W}$, respectively.

3.1.1 Supercritical CO_2 cycle

According to the energy and exergy balance relationships mentioned, the energy and exergy balance equations for the CO_2 supercritical cycle with re-condensation are presented as follows.:

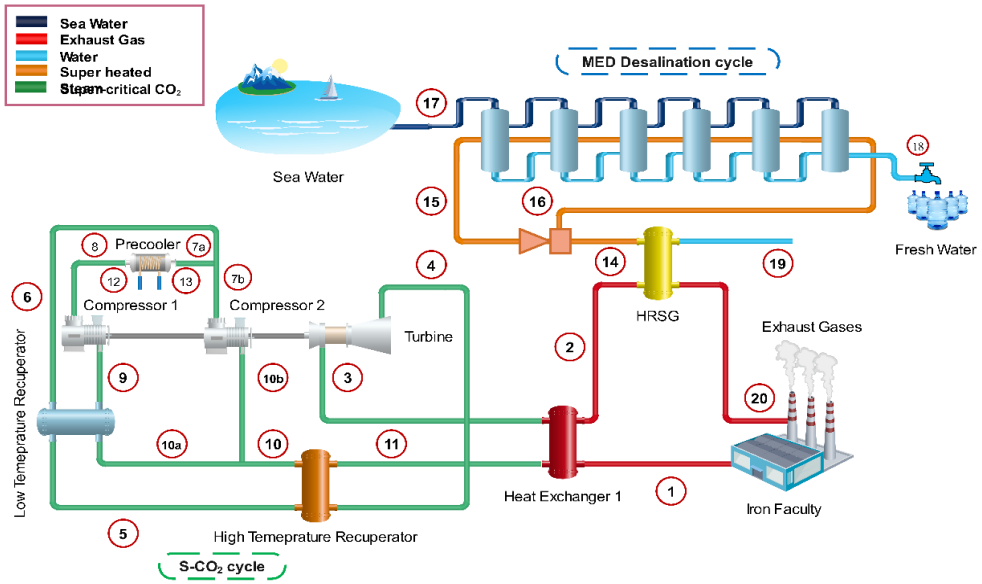

Fig. 1. The S-CO_2 and MED desalination system's schematic diagram.

Table 1. The summary of mass, energy, and exergy balance equations.

Component	Equations
Turbine	$\dot{W}_T = \dot{m}_3(h_3 - h_4),\ \eta_T = \frac{h_3 - h_4}{h_3 - h_{4s}}$ $\dot{E}_{D.T} = \dot{E}_3 - \dot{E}_4 - \dot{W}_T$
Compressor 1	$\dot{W}_{C1} = \dot{m}_9(h_9 - h_8),\ \eta_{c1} = \frac{h_{9s} - h_8}{h_9 - h_8}$ $\dot{E}_{D.C1} = \dot{E}_9 - \dot{E}_8 + \dot{W}_{C1}$
Compressor 2	$\dot{W}_{C2} = \dot{m}_{7b}(h_{10b} - h_{7b}),\ \eta_{c2} = \frac{h_{10bs} - h_{7b}}{h_{10b} - h_{7b}}$ $\dot{E}_{D.C2} = \dot{E}_{10b} - \dot{E}_{7b} + \dot{W}_{C2}$
HTR	$\varepsilon_{HTR} = \frac{T_4 - T_5}{T_4 - T_{10}}.(h_4 - h_5) = (h_{11} - h_{10})$ $\dot{E}_{D.HTR} = \dot{E}_4 + \dot{E}_{10} - \dot{E}_{11} - \dot{E}_5$
LTR	$\varepsilon_{LTR} = \frac{T_5 - T_6}{T_5 - T_9},\ \dot{m}_5(h_5 - h_6) = \dot{m}_9(h_{10a} - h_9)$ $\dot{E}_{D.LTR} = \dot{E}_5 + \dot{E}_9 - \dot{E}_6 - \dot{E}_{10a}$
Pre-cooler	$\dot{m}_{7a}(h_{7a} - h_8) = \dot{m}_{12}(h_{13} - h_{12})$ $\dot{E}_{D.pre-c} = \dot{E}_{7a} + \dot{E}_{12} - \dot{E}_8 - \dot{E}_{13}$
Mass balance relations	$\dot{m}_6 = \dot{m}_{7a} + \dot{m}_{7b},\ \dot{m}_{10} = \dot{m}_{10a} + \dot{m}_{10b},\ x = \frac{\dot{m}_{7b}}{\dot{m}_6}$ $\dot{m}_6 = \dot{m}_{10} = \dot{m}_{11} = \dot{m}_3 = \dot{m}_4 = \dot{m}_5$ $\dot{m}_{7a} = \dot{m}_8 = \dot{m}_9 = \dot{m}_{10a},\quad \dot{m}_{7b} = \dot{m}_{10b}$
Net Work	$\dot{W}_{net} = \dot{W}_T - \dot{W}_{C1} - \dot{W}_{C2}$
First law efficiency	$\eta_I = \frac{\dot{W}_{net}}{\dot{Q}}$
Exergy of heat transfer	$\dot{E}_Q = \dot{Q}_R \Sigma\left(1 - \frac{T_0}{T}\right)$
Second law efficiency	$\eta_{ex} = \frac{\dot{W}_{net}}{\dot{E}_Q}$

Table 2. Assumptions of supercritical CO_2 cycle modeling.

Parameter	Range
$T_0(°C)$	25
$P_0(bar)$	1.01
$P_4(bar)$	74
PR_C	3
$T_{max}(°C)$	550
$T_8(°C)$	35
$T_R(°C)$	800
$\eta_T(\%)$	0.9
$\eta_C(\%)$	0.85
$\varepsilon_{LTR\ \&\ HTR}$	0.86
$\dot{Q}_R(MW)$	600

The assumptions and the initial data used for modeling the S-CO_2 cycle are mentioned in Tabel 2.

3.1.2 Multi-effect desalination unit

The MED system is a prospective and cost-effective option for potable water production due to its lower energy consumption and lower operating temperature than competing technologies. For the MED unit modeling, a set of mass, salinity, and energy balance equations are formulated for each subsystem. Using T_{b_1} and T_{b_N} as the brine temperatures at the 1st and Nth effects, respectively, the temperature difference between the effects can be expressed as

$$\Delta T = \frac{T_{b_1} - T_{b_N}}{N-1}. \quad (4)$$

In addition, the temperatures of brine and water vapor at the subsequent effect are determined by

$$T_{b_{i+1}} = T_{b_i} - \Delta T, \quad (5)$$

$$T_{vi} = T_{bi} - BPE. \quad (6)$$

In the final equation, *BPE* represents the elevation of the boiling point. In addition, the brine cooldown temperature (T_i'), which is the sum of the non-equilibrium allowance (NEA_i) and the brine temperature (T_{b_i}), is expressed as

$$T_i' = T_{b_i} + NEA_i, \quad (7)$$

The energy balances for the steam ejector can be expressed as

$$M_m h_m + D_r h_g = (M_m + D_r) h_s \quad (8)$$

Additionally, Table 3 lists the thermodynamic equations for each effect of the MED unit.

For the 1st and 2nd to Nth effects, the formula of areas of heat transfer that are required for MED modelings given by

$$A_1 = \frac{M_s L_s}{U_{e1}(T_S - T_1)} \quad (9)$$

$$A_i = \frac{(D_{i-1} + D_{i-1}')L_{i-1}}{U_{ei}\Delta T_i}. \quad (10)$$

Here, U_e represents the total heat transfer coefficient of the ith effect, which can be calculated using

$$U_e = 1.9394 + 1.40562\times10^{-3}\times T_b - 2.07525\times 10^{-5}\times T_b^2 + 2.3186\times10^{-6}\times T_b^3 \quad (11)$$

3.2 Performance Evaluation

Using thermodynamics criteria, the performance of the proposed system is evaluated. In this regard, energy(η_I) and exergy efficiency (η_{ex}), are calculated under various system operating conditions. Calculating the energy and exergy efficiency are given by

$$\eta_I = \frac{\dot{W}_{net}}{\dot{Q}_{in}} \quad (12)$$

$$\eta_{ex} = \frac{\sum_{i=1}^{n_k} \dot{E}_{p_i}}{\dot{E}_{input}} \quad (13)$$

3.3 Optimization Procedure

Finding the most advantageous operating state in relation to a number of restrictions or important criteria is the aim of optimization. These include increasing positive objectives like net generated energy and performance efficiencies while reducing negative ones like carbon dioxide emissions and energy costs.

Table 3. Assumptions of supercritical CO_2 cycle modeling.

1st effect	Mass balance	$B_1 = F_1 - D_1$
	Salinity balance	$X_1 = \frac{F_1}{B_1} X_f$
	Energy balance	$M_m L_m = D_1 L_1 + F_1 C_P (T_1 - T_F)$
2 to N effect	Mass balance	$B_i = B_{i-1} + F_i - D_i$
	Salinity balance	$X_i = \frac{F_i}{B_i} X_f + \frac{B_{i-1}}{B_i} X_{i-1}$
	Energy balance	$(D_{i-1} + D'_{i-1}) L_{i-1} = D_i L_i + F_i C_P (T_i - T_F) + B_i C_P (T_i - T_{i-1})$

Table 4. Variables used in optimization.

Tournament size	Selection process	Probability of mutation	Probability of crossover	Maximum Number of generations	Population size
2	Tournament	0.01	0.85	600	500

4. Results

In this part, the findings of the modeling that were supplied in section 3 are shown. After evaluating the correctness of the generated model for each individual subsystem first, the results of the parametric research and optimization are then presented.

4.1 Model validation

In order to validate the results of CO_2 cycle modeling, the results available in the technical literature have also been used. For this purpose, the results of Sarkar et al.[15] have been used for comparison. Table 5(a) and 5(b) shows the results of the current modeling and the results of Sarkar's work. To compare the minimum and maximum temperature parameters of the cycle, the maximum pressure ratio has been used and the results are the optimal pressure ratio, thermal efficiency and the percentage of flow passing through the DWH, which is in good agreement with the results in the fan literature.

Table 5(a). Comparison of the present results and the results of Sarkar et al [15].

Parameters			PR_{opt}	
T_{min}(℃)	T_{max}(℃)	P_{max}(bar)	Present work	Ref [15]
32	550	200	2.641	2.64
32	550	300	3.864	3.86
32	750	200	2.65	2.65
32	750	300	3.942	3.94
50	550	200	2.392	2.40
50	550	300	2.795	2.80
50	750	200	3.076	2.88
50	750	300	3.102	3.08

Table 5(b). Comparison of the present results and the results of Sarkar et al [15].

y_{opt}		η_{Th}	
Present work	Ref [15]	Present work	Ref [15]
0.3338	0.334	41.18	41.18
0.3552	0.355	43.33	43.32
0.2086	0.223	46.12	46.07
0.2815	0.281	49.84	49.83
0.1839	0.184	36.7	36.71
0.2535	0.254	38.93	38.93
0.1111	0.109	43.56	43.50
0.1759	0.175	45.28	45.28

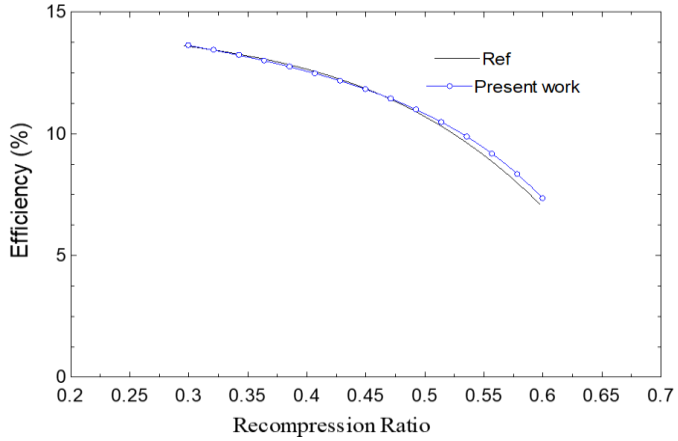

Fig. 2. Comparison of efficiency of CO_2 system with Shubnam Banik et al. [16].

Table 6. Comparison of the present MED model with a real plant.

Design conditions	Present Model	Real plant [17]
Effect numbers	6	6
Motive steam rate (kgs^{-1})	21.20	21.20
The pressure of motive steam (bar)	25	25
Minimum temperature of brine (°C)	42.8	42.8
Top brine temperature (°C)	61.80	61.80
Seawater temperature (°C)	30	30
Performance indicators		
Desalinated water (kg/s)	188.24	184.4
Gain output ratio	8.78	8.6

Also, the Fig. 2 shows the study of the efficiency of the first law in the work of Shubnam Banik et al. [16] with the data obtained from modeling. According to Fig.2, it is clear that the results are in good agreement with the reference results.

The MED unit model is validated by comparing it to the data of an actual plant, as shown in Table 6. It can be observed that nearly identical results are obtained for identical design parameter values, indicating the accuracy of the current model.

4.2 Parametric study

Considering that the accuracy of the modeling done for the components of the cycle was investigated, we will examine the cycle in general. In this section, we examine the effect of important parameters on cycle performance. Fig. 3 shows the effect of Rankine cycle pressure ratio on cycle efficiency. According to this figure, it is clear that by increasing the pressure ratio from 2 to 5, the evaporator pressure changes from 10,000 to 30,000 and the efficiency also increases from 23% to 34% due to the increase of input enthalpy in the turbine. Also, this efficiency increase occurs for the second law as well, in such a way that the efficiency increases from 22 to 31.9 %.

Figure 4 shows the effect of Rankine cycle pressure ratio on turbine work and total power. With the increase in the pressure ratio, it is clear that the output work of the turbine and the total work increases. Also, according to Fig. 5, it is clear that the input work to the pump also increases because it has to pump the fluid to a higher pressure. The increase in the input work of the pump is from 0.12 to 0.36, which is insignificant compared to the increase in the output work of the turbine from 1.1 kW to 1.5 kW and does not reduce the total work.

Figure 6 shows the effect of turbine inlet temperature on pump input power and turbine output power. According to this figure, it is clear that with the increase in the turbine inlet temperature, due to the increase in the turbine inlet enthalpy, the work output of the cycle increases from 1.43 to 1.49 kW and the cycle efficiency increases from 34.2 to 35.6 %, and the reason for this increase in efficiency is also because the work of the turbine increases and the input work of the pump decreases.

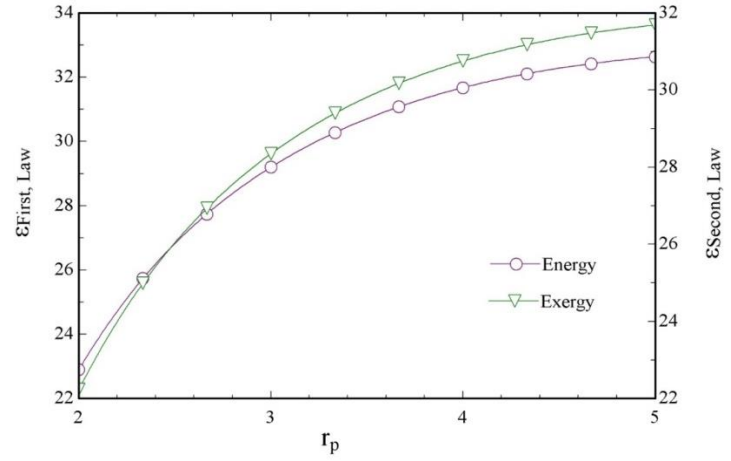

Fig. 3. The effect of Rankine cycle pressure ratio on cycle efficiency.

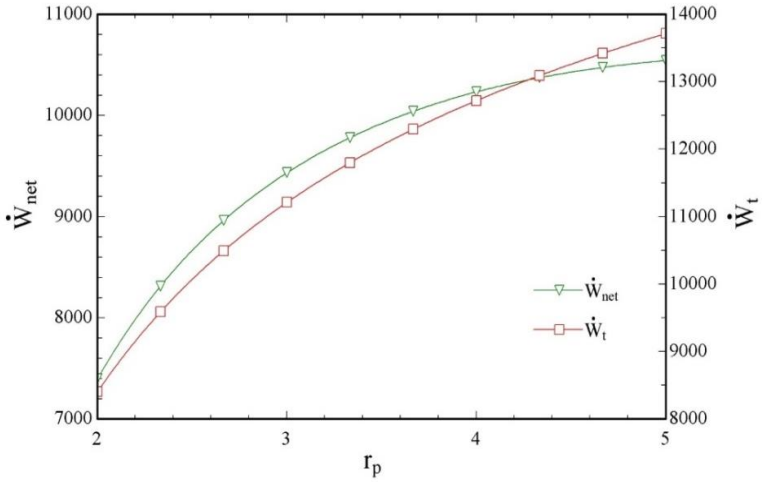

Fig. 4. The effect of Rankine cycle pressure ratio on turbine work and total power.

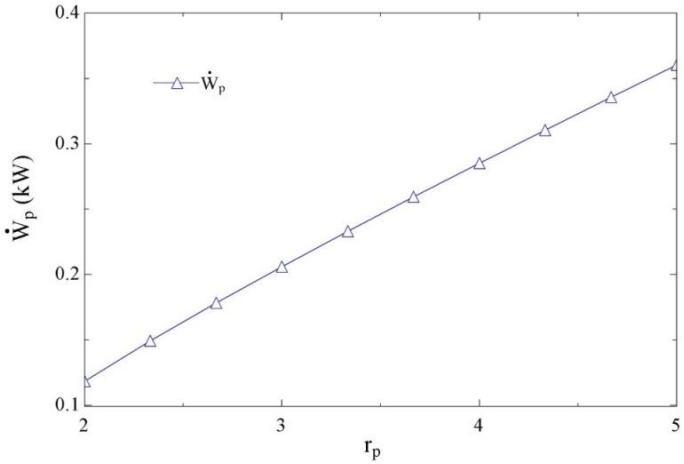

Fig. 5. The effect of Rankine cycle pressure ratio on pump work.

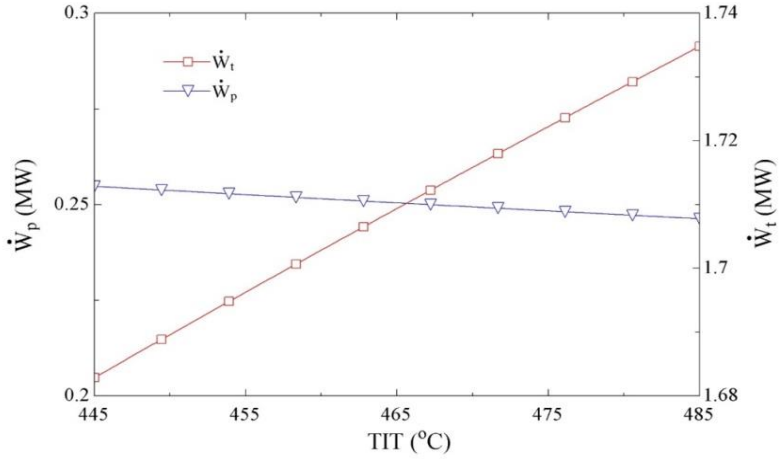

Fig. 6. Effect of turbine inlet temperature on pump input power and turbine output power.

Figure 7 shows the effect of recuperator efficiency on cycle efficiency and total output power and Fig. 8 shows the effect of recuperator efficiency on turbine power and pump power. According to these figures, it is clear that by increasing the efficiency of the recuperator from 70% to 95%, the efficiency of the first law reaches from 28.1% to 35.9%, and the total production power increases from 1.17 to 1.5 kW. According to these figures, with the increase in the efficiency of the recuperator, the output power of the turbine and the input power of the pump also increase, but the increase in the output power of the turbine is more than the input power of the pump, and the total output power increases.

Figure 9 shows the effect of the temperature of the exhaust gases of the recycling system on the cycle efficiency and the total output power, and Fig.10 shows the effect of the temperature of the exhaust gases from the recycling system on the recycled heat in the cycle and the turbine production power. By increasing the temperature of the exhaust gas by 150 degrees, it is clear that 2 MW of recycled heat can be obtained. Also, in this regard, the output work of the turbine has increased by 0.8 kW and increases the efficiency of the whole cycle by 31.5% to 37%.

The influence of the number of MED effects in the fresh water production is demonstrated in Fig. 11. According to the figure, as the number of effects increases from 3 to 14, the rate of fresh water produced increases more than 3 kg/s, which is considerable

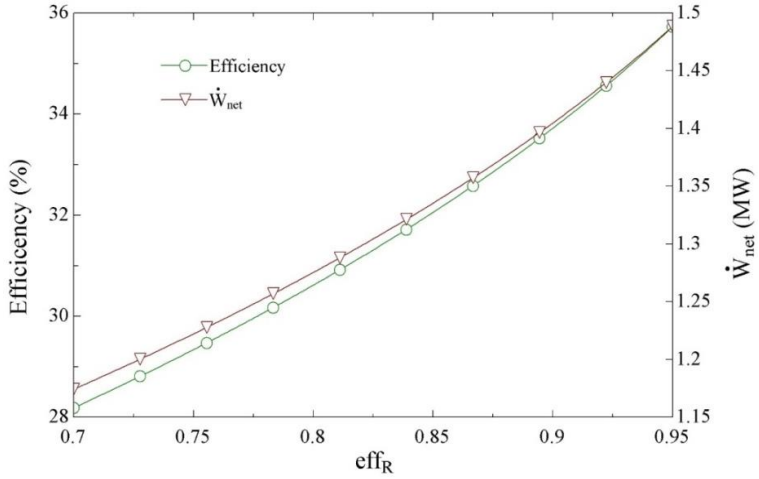

Fig. 7. The effect of recuperator efficiency on cycle efficiency and total output power.

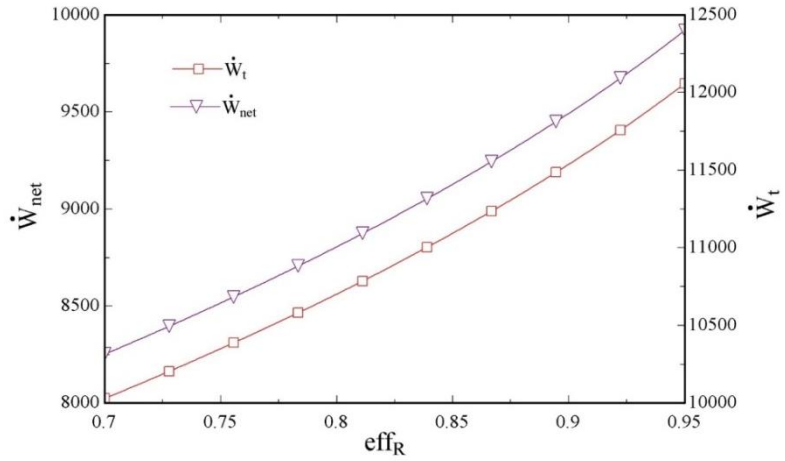

Fig. 8. The effect of recuperator efficiency on turbine power and pump power.

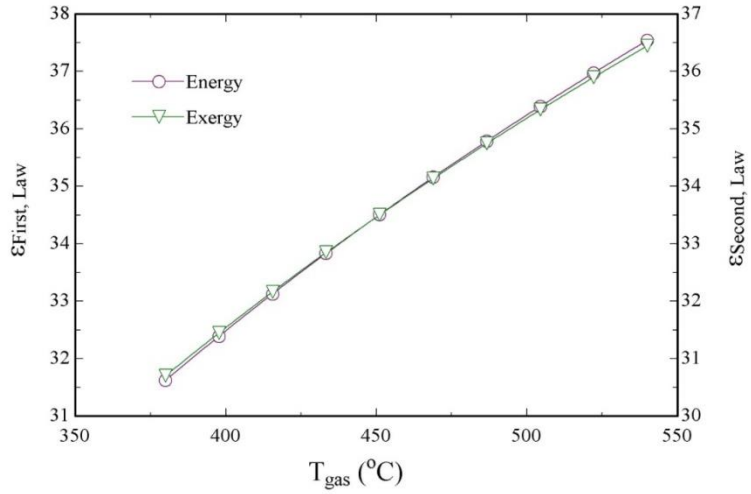

Fig. 9. The effect of the exhaust gas temperature of the recycling system on the cycle efficiency and total output power.

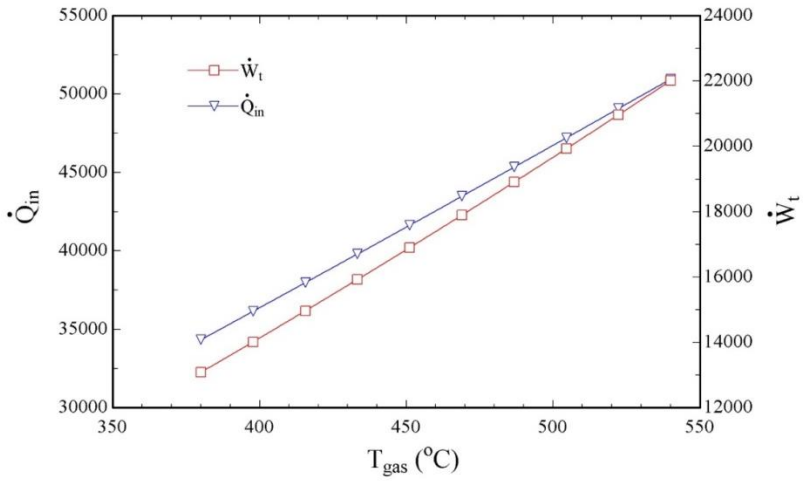

Fig. 10. The effect of the temperature of the exhaust gases from the recycling system on the recycled heat in the cycle and the production power of the turbine.

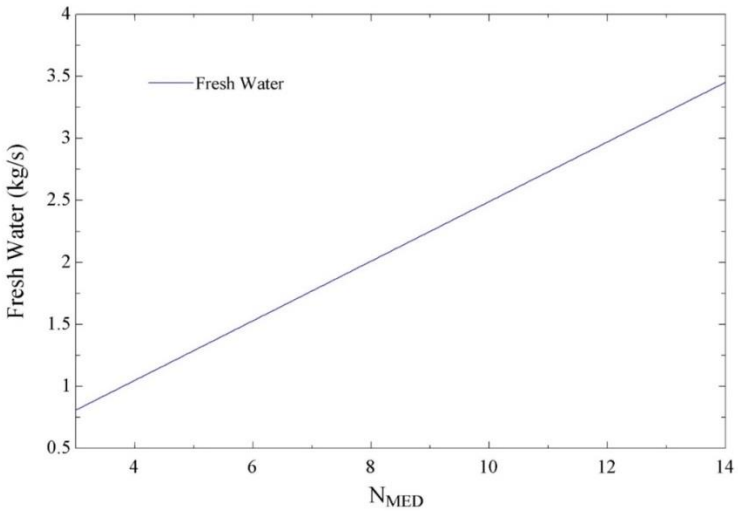

Fig. 11. The variation of fresh water with the number of MED effects.

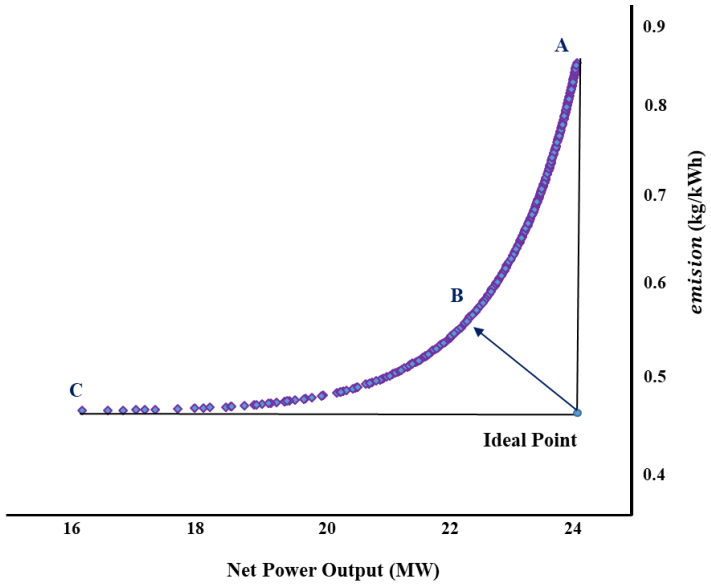

Fig. 12. Two-dimensional Pareto frontier diagram of net power output and emission.

4.3 Optimization

Figure 12 shows the optimization Pareto diagram for the system. The y-axis of this chart shows the pollution and the x-axis shows the net production work that should be minimized and maximized, respectively. At the optimal point, the system has emissions of 0.52 and net power output of 22100 (kWh).

5. Conclusions

This study aims to provide a hybrid system for recovering waste heat in steel facilities in different working conditions with the help of supercritical CO_2 cycle. The results obtained from the present study are as follows:

- At the optimal point, the system has emissions of 0.52 and net power output of 22100 kWh.
- System efficiency is 38.56% and carbon dioxide emission is 0.510 tons/MWh.
- By increasing the temperature of the exhaust gas output by 150 ℃, it is clear that 2 MW of recycled heat can be obtained. Also, in this regard, the output work of the turbine has increased by 0.8 kW and increases the efficiency of the whole cycle by 31.5% to 37%.

Reference

[1] Zetterholm J, Ji X, Sundelin B, Martin PM, Wang C. Dynamic modelling for the hot blast stove. Appl Energy 2017;185:2142–50. https://doi.org/10.1016/J.APENERGY.2016.02.128.

[2] Açikkalp E, Aras H, Hepbasli A. Advanced exergy analysis of an electricity-generating facility using natural gas. Energy Convers Manag 2014;82:146–53. https://doi.org/10.1016/J.ENCONMAN.2014.03.006.

[3] Boyaghchi FA, Molaie H. Sensitivity analysis of exergy destruction in a real combined cycle power plant based on advanced exergy method. Energy Convers Manag 2015;99:374–86. https://doi.org/10.1016/J.ENCONMAN.2015.04.048.

[4] Anvari S, Khoshbakhti Saray R, Bahlouli K. Employing a new optimization strategy based on advanced exergy concept for improvement of a tri-generation system. Appl Therm Eng 2017;113:1452–63. https://doi.org/10.1016/J.APPLTHERMALENG.2016.11.146.

[5] Dostal V, Hejzlar P, Driscoll MJ. The Supercritical Carbon Dioxide Power Cycle: Comparison to Other Advanced Power Cycles. Http://DxDoiOrg/1013182/NT06-A3734 2017;154:283–301. https://doi.org/10.13182/NT06-A3734.

[6] Milani D, Luu MT, McNaughton R, Abbas A. Optimizing an advanced hybrid of solar-assisted supercritical CO2 Brayton cycle: A vital transition for low-carbon power generation industry. Energy Convers Manag 2017;148:1317–31. https://doi.org/10.1016/J.ENCONMAN.2017.06.017.

[7] Zhao D, Xue J, Li S, Sun H, Zhang Q dong. Theoretical analyses of thermal and economical aspects of multi-effect distillation desalination dealing with high-salinity wastewater. Desalination 2011;273:292–8. https://doi.org/10.1016/J.DESAL.2011.01.048.

[8] Chen Q, Burhan M, Shahzad MW, Ybyraiymkul D, Akhtar FH, Li Y, et al. A zero liquid discharge system integrating multi-effect distillation and evaporative crystallization for desalination brine treatment. Desalination 2021;502:114928. https://doi.org/10.1016/J.DESAL.2020.114928.

[9] Tahir F, Al-Ghamdi SG. Integrated MED and HDH desalination systems for an energy-efficient zero-liquid discharge (ZLD) system. Energy Reports 2022;8:29–34. https://doi.org/10.1016/J.EGYR.2022.01.028.

[10] Tahir F, Al-Ghamdi SG. CFD analysis of evaporation heat transfer for falling films application. Energy Reports 2022;8:216–23. https://doi.org/10.1016/J.EGYR.2021.11.096.

[11] Chitgar N, Emadi MA. Development and exergoeconomic evaluation of a SOFC-GT driven multi-generation system to supply residential demands: Electricity, fresh water, and hydrogen. Int J Hydrogen Energy 2021;46:17932–54. https://doi.org/10.1016/J.IJHYDENE.2021.02.191.

[12] Aguilar-Jiménez JA, Velázquez N, López-Zavala R, Beltrán R, Hernández-Callejo L, González-Uribe LA, et al. Low-temperature multiple-effect desalination/organic Rankine cycle system with a novel integration for fresh water and electrical energy production. Desalination 2020;477:114269. https://doi.org/10.1016/J.DESAL.2019.114269

[13] Marques JGO, Costa AL, Pereira C. Thermodynamic study of a novel trigeneration process of hydrogen, electricity and desalinated water: The case of Na-O-H thermochemical cycle, SCWR nuclear power plant, and MED desalination installation. Energy Convers Manag 2020;209:112648. https://doi.org/10.1016/J.ENCONMAN.2020.112648.

[14] Bejan A, Tsatsaronis G. Thermal design and optimization. John Wiley & Sons; 1996.

[15] Sarkar J, Bhattacharyya S. Optimization of recompression S-CO2 power cycle with reheating. Energy Convers Manag 2009;50:1939–45. https://doi.org/10.1016/j.enconman.2009.04.015.

[16] Banik S, Ray S, De S. Thermodynamic modeling of a recompression CO2 power cycle for low-temperature waste heat recovery. Appl Therm Eng 2016;107:441–52.

https://doi.org/10.1016/j.applthermaleng.2016.06.179.

[17] Moghimi M, Emadi M, Akbarpoor AM, Mollaei M. Energy and exergy investigation of a combined cooling, heating, power generation, and seawater desalination system. Appl Therm Eng 2018. https://doi.org/10.1016/j.applthermaleng.2018.05.092.